Mechanically resistant and sustainable cellulose-based composite aerogels with excellent flame retardant, sound-absorption, and superantiwetting ability for advanced engineering materials

He, Chenglin; Huang, Jianying; Li, Shuhui; Meng, Kai; Zhang, Liyuan; Chen, Zhong; Lai, Yuekun

2017

He, C., Huang, J., Li, S., Meng, K., Zhang, L., Chen, Z., & Lai, Y. (2017). Mechanically resistant and sustainable cellulose-based composite aerogels with excellent flame retardant, sound-absorption, and superantiwetting ability for advanced engineering materials. ACS Sustainable Chemistry & Engineering, 6(1), 927-936. doi:10.1021/acssuschemeng.7b03281

https://hdl.handle.net/10356/106130

https://doi.org/10.1021/acssuschemeng.7b03281

Mechanical resistant and Sustainable Cellulose-based Composite Aerogels with Excellent Flame Retardant, Sound-absorption and Super-antiwetting Ability for Advanced Engineering Materials

Chenglin He,[a1] Jianying Huang,[a1] Shuhui Li,[a] Kai Meng,[a] Liyuan Zhang,[b] Zhong Chen,[c] and Yuekun Lai[*,a,c]*

[a] National Engineering Laboratory for Modern Silk, College of Textile and Clothing Engineering, Soochow University, Suzhou 215123, P. R. China

[b] Department of Civil Engineering, The University of Hong Kong, Hong Kong, P. R. China

[c] School of Materials Science and Engineering, Nanyang Technological University, 50 Nanyang Avenue, Singapore 639798, Singapore

[1]These authors contributed equally in this work.

Corresponding Authors E-mail: yklai@suda.edu.cn

Abstract: The production of cellulose-based aerogels from the conversion of cheap and rich precursors using environmentally friendly techniques is a very attractive subject in materials chemistry. In this work, we reports a facile strategy to construct flame retardant, sound-adsorption and mechanical enhancement cellulose-based composite aerogels by the incorporation of aluminum hydroxide nanoparticles (AH NPs) into cellulose gels via an in-situ sol-gel process, followed by freeze-drying to coat AH NPs on cellulose composite aerogels (AH NPs@cellulose composite aerogels). The results demonstrated that the AH NPs homogeneous dispersion within cellulose aerogel, and the presence of AH NPs did not have a remarkable influence on the

homogeneous porous structure of cellulose aerogels when compared with cellulose aerogel prepared from the NaOH/urea/thiourea solution. The prepared composite cellulose aerogels showed excellent flame retardancy, the peak of heat release rate (PHRR) of the composite aerogels decreased significantly from 280 W/g of the control sample to 22 W/g, and total heat release (THR) of the composite aerogels decreased remarkably from 13.2 kJ/g to 1.6 kJ/g. Moreover, the incorporation of AH NPs composite aerogels exhibited remarkable mechanical properties, the compressive strength of the composite aerogels increased significantly from 0.08 MPa to 1.5 MPa. In addition, AH NPs composite cellulose aerogels have excellent sound absorption at high frequencies with a maximum sound absorption coefficient of 1. AH NPs composite cellulose aerogels have strong water and oil affinity. After immersing the samples in mixed silica nanoparticles, heptadecafluorononanoic, and fluoroalkyl silane solutions they became super-antiwetting, with a water contact angle (CA) larger than 150° and oil CA larger than 140°. In summary, this study provides a facile strategy to rationally construct flame retardant, mechanically robust, high-efficiency sound-adsorption and superamphiphobic cellulose-based composite aerogels, which have promising applications in the future as green engineering materials.

Keywords: aerogel, cellulose-based composite, flame retardant, sound-adsorption, superamphiphobicity

Introduction

Cellulose aerogels are ultralight three-dimensional porous materials, which combine the excellent properties of highly porous aerogels[1], such as high specific surface area, low density, low thermal conductivity, and high insulation, with the fantastic properties of sustainable biopolymers such as biodegradability and biocompatibility[2, 3]. Consequently, they have received widespread attention in the 21st century ascribed to their potential applications in waste-water treatment[4-7], tissue engineering[8, 9], and flexible devices[10,11], etc. Cellulose aerogel is considered one of the most promising heat insulating materials due to its abundant internal pores and good thermal insulation performance[12-15]. However, because of high porosity, they dispaly poor mechanical properties, such as poor toughness, low strength and high brittleness, limiting their utility for many commercial applications. In addition, cellulose aerogels is easy to ignite, which is major hindrance to its wide usages in

many important areas such as light weight engineering materials or devices. Thus, any improvements in their mechanical and flame retardant properties while maintaining their unique characteristics represent important advances towards practical applications.

To solve the mechanical friability of aerogels, a possible way is to consolidate the pregelation process by storing the original cellulose solution at a pre-gelation temperature that leads to the formation of network units with stronger cross-linking[16, 17]. However, the conventional pregelling process is very time consuming and the improvement in mechanical property is also quite limited. In contrast, incorporation of reinforcement additives is a relatively easy technique for improving the mechanical property of cellulose aerogels. The reported wad include graphene[18-21], clay[22-24], organic polymers[25-28], cellulose whisker[29], metal nanoparticles or other related mixtures[30, 31]. However, the improvement in the mechanical property is insufficient, robust aerogels have to come with other excellent performances simultaneously in order to be used as multifunctional green engineering materials. For example, the fire-resistant, sound-absorption and superamphiphobic abilities are also important characters for the practical application of building materials. To improve the fire-resistant performance of cellulose aerogels has been the main topic of great number of interesting scientific studies. One of the effective strategies for this aim is the inclusion of additives, including graphene oxide, magnesium hydroxide, montmorillonite and sepiolite, formed in-situ[32] or incorporated[33] in the cellulose aerogels. Synerygistic additives can form a dense protective layer on the surface, which could isolate oxygen to achieve flame retardant effect.

Aluminum hydroxide (AH) is a widely used inorganic filler with good flame retardancy and smoke suppression abilities. It is inert, non-toxic, and can be produced without secondary pollution, so it is widely known as pollution-free flame retardant. Aluminum hydroxide has not only a high whiteness value, but also excellent color index. During the thermal degradation process, aluminum hydroxide undergoes endothermic dehydration, forming a dense and stable protective Al_2O_3 layer on the surface, and releasing moisture to the gas phase at the same time, protecting the underlying matrix[34-36]. The flame retardancy increases with the decrease of the aluminum hydroxide particle size. Therefore, aluminum hydroxide nanoparticles is commonly used in nanometer flame retardants to improve its flame retardant efficiency.

This work is focused on the improvement of the mechanical and flame retardant properties of cellulose aerogels. In order to achieve green sustainable development, we will waste cotton as a source of cellulose, so as to give full play to the effective value of resources and to relieve environmental pollution crisis. we propose a facile approach to prepare cellulose aerogels by dissolution and coagulation of cellulose from aqueous NaOH/urea/thiourea solution as highly effective templates for the non-agglomerated growth of aluminum hydroxide nanoparticles (AH NPs). By coagulating in ethyl alcohol and further freeze-drying, robust cellulose aerogels with a low density, high-efficiency sound-adsorption, excellent flame retardancy, and

good mechanical properties can be created for versatile applications, such as the domestic devices, aerospace, automotive, and building industries.

Experimental

Materials. Waste cotton were provided by Suzhou Yintong Cotton Co., Ltd. Sodium hydroxide (NaOH), urea, thiourea, aluminum chloride hexahydrate, ammonia, methyl blue, methyl orange and oil red were purchased from Sinopharm Chemical Reagent Co., Ltd. (Shanghai, China) Heptadecafluorononanoic acid (HFA) came from J&K Scientific Ltd., SiO_2 nanoparticles be supplied by Shanghai Macklin Biochemical Co., Ltd. Fluoroalkylsilane was provided by Sigma-Aldrich, Co., Ltd. (USA) All chemical reagents are analytical-grade and used as received without further purification.

Preparation of AH NPs@cellulose composite aerogels. The schematic illustration of the preparation process for AH NPs@cellulose composite aerogels is shown in Figure 1. Initially, cylindrical shaped pieces of cotton fibers were washed with deionized water, and then dried in vacuum at 60°C for 12 h. After that, the dried cotton was smashed into pieces, and 100 g of aqueous solution with 7 wt% NaOH, 9 wt% thiourea and 9 wt% urea was pre-cooled to -12°C with a refrigerator for 2 h, which is proposed as a promising candidate for cellulose dissolution owing to its low cost, nontoxicity, and environmental friendliness. Subsequently, 2 g (2 wt%) of cotton fibers was immediately added to the pre-cooled solvent and mechanically stirred for 0.5 h under room temperature conditions. Then the cellulose solution was poured into molds and coagulated in absolute ethanol for 12 h at room temperature forming cellulose hydrogel. The resulting cellulose hydrogels were rinsed with deionized water to remove reaction residues. Then, cellulose hydrogels were immersed into the aluminum chloride solution of various concentrations (0.25, 0.5, 0.75, and 1.0 mol/L) for 12 h. The obtained cellulose hydrogels containing Al^{3+} were dipped into excess ammonia to synthesize AH NPs. The obtained cellulose nanocomposite gels were soaked in deionized water and absolute ethanol to remove the residual chemical reagents. Finally, the samples were freeze-dried in a vacuum freeze dryer at -50°C for 48 h. The removal of water phase in the composite hydrogel resulted in the formation of a three-dimensional porous AH NPs@cellulose composite aerogel. Aerogels with different AH NPs loadings were coded as CA1, CA2, CA3, and CA4 corresponding to 0.25, 0.5, 0.75, and 1.0 mol/L of aluminum chloride in order to distinguish with the aerogel without AH NPs, which was coded as CA0.

Preparation of Superamphiphobic AH NPs@cellulose composite aerogels. Superamphiphobic AH NPs@cellulose composite aerogels was obtained via a developed facile soaking process in fluorine-containing solution[37]. In briefly, 200 μL of FAS was added dropwise to 2.5 mL of ethanol solution, and then slowly added dropwise to a solution of 0.25 g of HFA in 10 mL of ethanol with vigorous stirring. Then, 27 μL of deionized water was added dropwise to the mixture and stirred under ambient conditions for 2 hours. Then the prepared solution was added with 0.1 g of silica nanoparticles. Subsequently, the AH NPs@cellulose composite aerogels was immersed in this solution for 2 h. Finally, the AH NPs@cellulose composite aerogels was dried at 150°C for 1 h.

Characterization. The crystal phases of the prepared samples were characterized by an X-ray diffractometer with CuKα radiation (XRD, Philips, X'pert-Pro MRD). The samples were blended with KBr and pressed into a disk, which were then examined in range of 400-4000 cm^{-1} by a Nicolet 5700 Fourier transform infrared (FTIR) spectrometer equipped with a single reflection ATR system. The microstructure and elemental analyses of the aerogels were investigated using a TM3030 scanning electron microscopy equipped with an energy-dispersive X-ray spectroscope (EDX). The mechanical properties of aerogels were conducted on an Instron 5967 universal testing machine with a crosshead speed of 1 mm/min until a maximum load of 4 kN was applied. TGA testingwas measured by a Diamond TG/DTA (TA instruments, USA) under nitrogen atmosphere with a heating rate of 10°C/min in a stream of N_2 flowing at 50 mL/min. AH NPs content of the composite aerogel was calculated by weighing the sample and neat cellulose aerogel. The aerogel density is calculated by measuring the sample volume and weigh. Flame retardancy was assessed by lighting the aerogel with an alcohol lamp, and by a micro-scale combustion calorimeter (MCC) for quantitative analysis. A sample of about 5 mg were heated from ambient temperature to 800°C with a heating rate of 1°C/s in a stream of N_2 flowing at 80 mL/min. Then the volatiles were mixed with a stream of O_2 (20 mL/min) prior to entering a 900°C combustion furnace. The smoke suppression of the cellulose aerogels and AH NPs@cellulose composite aerogel samples were tested by using an NBS smoke density test chamber according to the ISO 5659-2 testing standard in terms of flameless combustion mode at 560°C for 500s, with max radiant heat of 25 kW/m^2 and sample of 80 × 80 × 5 mm^3. Sound-absorption tests were carried out in a SW477 impedance tube (Beijing China prestige Sound Technology Co. Ltd., China). The water and oil contact angles were measured by an optical contact angle meter system (Krüss DSA100) with 6 μL droplets. The neat cellulose aerogel without AH NPs regarded as control samples were also measured using the above-described equipment and methods.

Results and discussion

Characterization of AH NPs@cellulose composite aerogels

Figure 2a showed the XRD pattern of AH NPs@cellulose composite aerogels and cellulose aerogels. The diffraction peaks at 2θ = 12.2°, 20°, and 21.8° for (11-0), (110), and (200) planes are characteristic of cellulose II crystal. The peaks located at 18.8°, 20.3°, 31.7°, 40.7°, 45.4°, and 56.5°, corresponding to the (001), (020), (121), (201), (-221), and (051) lattice planes, respectively, indicate the successful synthesis of the AH NPs. Furthermore, there is no signal of the disappearance on the characteristic peaks of cellulose and AH NPs, which indicates no interference in structure formation between the two components. The coexistence of the cellulose and AH NPs peaks indicated that the AH NPs@cellulose composite aerogel was prepared successfully. Figure 2b showed the FT-IR spectra of cellulose, cellulose aerogels and AH NPs@cellulose composite aerogels. New adsorption band at 3647 and 3543 cm^{-1} are usually found in all kinds of aluminum hydroxides, and they represent strong interactions between the hydroxyl groups and aluminum atoms,[38] confirming that the AH NPs were successfully synthesized. The adsorption at 1430.8 cm^{-1} was weak and even disappeared in the cellulose aerogels and AH NPs@cellulose composite aerogels, which is characteristic of the transition from cellulose I to cellulose II involving the change of the conformation of CH_2OH at C6 position in cellulose from trans-gauche (tg) to gauche-trans (gt). In addition, the unchanged characteristic absorption bands of cellulose at about 3438, 2902 and 1062 cm^{-1} suggested that the main composition of the cotton fibers remained after dissolution.

The surface morphology of cellulose aerogel and AH NPs@cellulose composite aerogel were characterized by SEM as shown in Figure 3. The cellulose aerogel displayed a homogeneous porous structure (Figure 3a). The pore structure resulted from the sublimation of frozen water during the freeze-drying process. The AH NPs@cellulose composite aerogel also exhibited a homogeneous porous structure even with the incorporation of a large amount of AH NPs (Figure 3b-e), which revealed that AH NPs did not have a remarkable influence on the homogeneous porous structure of cellulose aerogels by this in situ synthesis method. After in situ synthesis, some AH NPs with diameters about 50-200 nm appeared on the surface of the composite aerogel CA4 as shown in Figure 3f. The nanocomposite elemental compositions of the AH NPs@cellulose composite aerogel was further examined by EDS analysis. As shown in Figure 4, EDS spectra showed that the main elements in the composite aerogel are Al, O, and C, which verified the aluminum hydroxide nanoparticles are uniformly distributed in the nanocomposite aerogels. Therefore, the presence of aluminum hydroxide nanoparticles does not affect the three-dimensional porous structure of cellulose aerogels.

Mechanical properties of AH NPs@cellulose composite aerogels

The mechanical properties of porous aerogels are crucial for many applications. As demonstrated in Figure 5a, the celloluse aerogels completely crushed under a load of 200 g. Compared to CA0, in the presence of a small amount of aluminum hydroxide, the AH NPs@cellulose composite aerogel CA1 compression performance has been greatly improved as show

Figure 5b. At the same time, in the presence of a large amount of aluminum hydroxide, the AH NPs@cellulose composite aerogels CA4 almost did not show any deformation under a load of 200 g as show Figure 5c. The compressive stress-strain curves of the composite aerogels are shown in Figure 5d. At the beginning, the stress-strain curves are relatively steepwhich means smaller amount of deformation with the incremental stress. The compressive strength increases with the increment of AH NPs content. For the cellulose aerogel, the compressive strength is 0.08 MPa, however, the compressive strength reached to 1.5 MPa for the composite aerogel CA4, increased by about 18 times. These results revealed that the AH NPs played a vital role in the enhancement of the mechanical strength of cellulose aerogel. As described above, AH NPs were uniformly distributed in cellulose aerogels to form a hierarchical composite nanostructures. Due to the interconnected porous structure of the cellulose aerogels, the external stress of the cellulose aerogels will lead to bending deformation of the single pores. For pure cellulose aerogels, stress is condensed in the curved region, resulting in rapid propagation of cracks across the cellulose aerogels, leading to the breakage of the cellulose aerogels. Otherwise, for the cellulose aerogels with AH NPs uniformly distributed in the cellulose matrix, the concentrated stress could be effectively scattered and dissipated.[39, 40] Moreover, the uniformly distributed AH NPs with an appropriate size in the cellulose matrix were believed to act as buffer substances to inhibit or change the extension direction of tiny cracks. Meanwhile, the energy originated from the external stress was absorbed, therefore the structural fracture of the cellulose matrix could be effectively avoided. At the same time, the introduction of AH NPs resulted in a more condensed structure to avoid collapse of the three-dimensional nanopore structure, resulting in higher compressive strength.[41] Due to the enhanced compressive strength, the AH NPs@cellulose composite aerogels are potentially useful as heat insulating material with high mechanical strength.

Thermal stability of AH NPs@cellulose composite aerogels

In view of the importance of thermal stability for the practical application of heat insulating materials, the thermal decomposition behavior and the amount of residues of the composite aerogel and cellulose aerogel are obtained from TG test under N_2 atmosphere with a heating rate of 10°C/min. The TG and DTG curves are displayed in Figure 6 a and b. As the main factors to affect the thermal stability property of composite materials, the density and AH NPs content of aerogels are measured and shown in Figure 6c and d. As shown in Figure 6, a slight weight loss occurred at relatively low temperature (<100°C) for both samples due to the loss of moisture. Compared with pure cellulose aerogel, the decomposition temperatures of AH NPs@cellulose composite aerogels are reduced. Sample CA1 was rapidly decompose from 238°C. The initial thermal degradation temperatures of CA2, CA3, and CA4 are 246, 215, and 208°C, respectively, which is similar to CA1. The reason is mainly due to the decomposition of AH NPs. The degradation of AH NPs and cellulose main chain occurred in the initial thermal degradation stage from about 210 to 330°C. The thermal properties of AH NPs@cellulose composite aerogels are not improved compared with pure cellulose aerogel before 330°C. The second stage is the decomposition of cellulose backbone

from about 330 to 400°C. The thermal stability of AH NPs@cellulose composite aerogels is significantly increased in this process. When the temperature reached 400°C, the TG curves become flat, but the content of residues is notably different for all the samples. The residues of CA0, CA1, CA2, CA3, and CA4 at 800°C are 8.95%, 20.13%, 35.21%, 39.67, and 47.69%, respectively. Compared with CA0, the amount of residues gradually increased. Because AH NPs are uniformly dispersed in the cellulose aerogels, the composite aerogels can form a continuous and dense network structure protective layer with the gradual increase of AH NPs content. When it is thermally decomposed at high temperature, the protective layer could effectively prevent further thermal decomposition of cellulose andeffectively delay the loss of quality.[42] Therefore, the AH NPs can enhance the charring contents in cellulose aerogel system. This is mainly ascribed to the decomposition of AH NPs, which generate alumina overlapping with the pyrolysis of the cellulose. It can be seen that the theoretical weight of residue for AH NPs@cellulose composite aerogels was obviously higher than that of cellulose aerogel. This may be attributed to the fact that alumina forms a dense barrier on the surface of cellulose to protect the cellulose from further combustion.

Flame retardancy of AH NPs@cellulose composite aerogels

In order to investigate the flame retardancy performance of the composite aerogels, the aerogels were ignited and the combustion velocity was calculated. As show in Figure 7a, the cellulose aerogel was ignited quickly with rapid flame propagation and burned completely after removal of the flame. However, the AH NPs@cellulose composite aerogels were immediately self-extinguished after removal of the flame (Figure 7b), most samples remained intact after the test. The results indicated that the incorporation of AH NPs could efficiently increase the flame retardancy of the cellulose aerogel.

The micro-scale combustion calorimeter (MCC) was applied to further quantitatively analyze the flammability of the AH NPs@cellulose composite aerogels. The curves of the heat release rate (HRR) is presented in Figures 7c, and the corresponding data are listed in Table 1, including peak of heat release rate (PHRR), ignition time (IT), total heat release (THR) and corresponding time (TI_{PHRR}), temperature (T_{PHRR}). Cellulose aerogel (CA0) has a sharp HRR curve, with a highest PHRR value of 280 W/g. In contrast, the sharp heat release peak for CA1, CA2, CA3 and CA4 with much smaller PHRR values of 100 W/g, 61 W/g, 45 W/g and 22 W/g, decreased by 64.3%, 78.2%, 83.9% and 92.1%, respectively. For the sharp peak of CA0, it burns severely without any retardancy. For gradually reduced peaks of CA1-4, because AH NPs are decomposed and the generated alumina can reduce the heat from the flame zone from reaching the sample. It has also inhibited the inner pyrolysis products from being released out. THR is used to measure the total heat release of material during combustion, which is determined by the flammable decomposition products. Table 1 illustrated the THR values of cellulose aerogel and AH NPs@cellulose composite aerogels. The THR value of CA0 was 13.2 kJ/g, while the corresponding values for CA1, CA2 and CA3 were 5.8 kJ/g, 4.7 kJ/g and 3.1 kJ/g, respectively. Especially for CA4 sample, the THR value was only 1.6 kJ/g. The

results of total heat release exhibited AH NPs provided a positive influence for flame retardancy property of cellulose composite aerogels.

Fire growth index (FGI) and fire performance index (FPI)

In order to further clearly evaluate the fire hazard, we study the fire performance index (FPI) (Figure 7d) and the fire growth index (FGI) (Figure 7e) after MCC. The fire growth index (FGI) is the ratio of the peak heat release rate (PHRR) of a material to the peak time, which reflects the size of the materials on the thermal reaction ability, and a greater FGI value means it will be much quicker for the fire to grow once was lit and there is a short duration to reach PHRR (greater fire hazard). The FPI refers to the ratio between the time to ignition (TTI) of the material and the value of the peak heat release rate (PHRR). The FPI refers to reach after a fire flashover need time. When FPI is smaller, the easier material after fire flashover occurred, the greater the fire risk. Therefore, with the aim to improve the fire safety index of specific material, it requires not only low FGI value but also high FPI value. Figure 7d,e respectively shows the FPI and FGI values of all samples. It is clearly seen that the FPI much increased and the FGI much decreased with the incorporation of AH NPs, which indicates that the AH NPs reveal good flame retardancy on cellulose aerogel composites. Furthermore, the values of FPI first increased and then decreased with the content of AH NPs increasing, and the values of FGI follow an opposite trend to FPI. Among all samples, CA4 shows the highest FPI and lowest FGI, which indicate that a high proportion of AH NPs can provide higher safety rank than others.

Smoke suppression

The smoke suppression characteristics of material refer to the maximum density of smoke (DS) released during flameless combustion. In the general NBS measurement, the photometric system was used to quantify the density of released smoke by testing the transmission of light. The lower the DS value, the better the smoke suppression effect of the material. The main reason for the death of the fire is smoke, the greater the concentration of smoke when burning material, the more detrimental to fire rescue. It can be seen from the Figure 8 that the max smoke densities of samples CA0, CA1, CA2, CA3 and CA4 are 93.7, 50.8, 35.6, 18.9 and 9.7, respectively. Compared with CA0, the max smoke density of CA1, CA2, CA3 and CA4 decreased by 45.8%, 62%, 79.8% and 89.6%. These results demonstrate that AH NPs play a vital role in reducing the smoke concentration of cellulose aerogels.

Morphology of carbon residue

It is well known that the effective protection of the char layer can enhance the flame retardant performance during combustion. Figure S1 (Supplemental Information) shows the SEM images of the residue collected after the MCC. Figure S1a-e are low

magnification of CA0, CA1, CA2, CA3 and CA4 carbon residues, respectively. There is no obvious change of the morphology at the low magnification. The char residues after burning were presented in high magnification image in Figure S1f-j of CA0, CA1, CA2, CA3 and CA4. It can be seen from Figure S1f, the char has a fluffy structure for the sample CA0 filled without AH NPs, but as shown in Figure S1g-j, the char of AH NPs@cellulose composite aerogels is smooth and dense, which could separate the heat spread and prevent the oxygen from reaching the sample surface for further burning. At the same time, with the increase of AH NPs concentration, the composite aerogels material can form a continuous and dense protective layer without forming a crack which damages the flame retardant effect. The protective layer can be used as the insulating layer of the original polymer.[43] Metal oxide generated during decomposition showed high specific heat capacity, which contributed to the excellent heat absorption.[43] The metal oxides acted as a heat barrier during combustion, resulting in the inhibition of fire spread. Meanwhile, it can effectively enhance the thermal stability of char residues via catalytic reactions in the solid phase.[44] The EDS spectra and the results of the char for the AH NPs@cellulose composite aerogels is presented in Figure S2. It can be seen that carbon became the main element in the residues. This indicates during the thermal decomposition process of the AH NPs@cellulose composite aerogels, the AH NPs were degraded into metallic oxides, which results in the absorption of the decomposition products originating from the cellulose aerogel matrix. The adsorbed compounds transferred into carbon by catalytic action in the solid phase.[45]

Potential flame-retardant mechanism

On the basis of the above analysis, it is interesting to observe that the addition of AH NPs has obviously improved the thermal stability and fire retardancy of cellulose aerogels. The proposed mechanisms for the enhanced thermal- and flame-retardant behaviors of the materials are illustrated in Figure 9. First, the AH NPs is decomposing during the combustion process to carry abundant heat away, thereby lowering the surface temperature of the sample. At the same time, the process of decomposition releases plenty of water and will not produce toxic, flammable or corrosive gas, which has contributed to the reduction of the concentration of oxygen on the surface. After that, the porous metallic oxides, generated during the combustion process, not only retard the heat spread but also suppress the release of fuel from the solid phase to the combustion area.[45] After that, the nano-metal particles can form a continuous and dense network-structured protective layer without forming a crack that damages the flame-retardant effect, which can serve as a thermal insulation layer of the original polymer below the layer while isolating oxygen to prevent combustion.[46-49] Based on these facts, the flame-retardant properties of cellulose composites aerogel are greatly improved.

Sound-absorption of AH NPs@cellulose composite aerogels

The cellulose aerogels materials have good sound absorption or dissipation. The Figure 10 showed the sound absorption coefficient of the all cellulose-based aerogels under a high frequency range from 1000 Hz to 6000 Hz. The sound absorption coefficienct of all samples are high at high frequencies, the sound absorption one for CA0 is good in 3000–6000 Hz. CA1 has a great sound absorption effect in 2500–6000 Hz range with an obvious peak around 4800 Hz. By contrast, CA2 and CA3 did not show such peaks in this frequency range, but they all showed very good sound absorption. CA4 diaplayed a peak with the highest sound absorption coefficient (close to 1 at 3000 Hz). The results above were attributed to the high porosity and small pore size. In the case of high porosity, the diffuse refraction or reflection enhancement and the vibration of the hole wall are increased after the sound waves entered the porous material, and the sound waves are effectively attenuated. At the same time, the micropores and channel twists and turns cause increased friction and air viscosity consumption, thus improve the sound absorption performance. There is also a major factor in the reduction of the size of the aperture to increase the friction through the acoustic waves of the pores, so that the reflected sound energy is less. This verifies that the AH NPs@cellulose composite aerogels are promising candidate as sound absorbing engineering materials.

Superamphiphobic property of AH NPs@cellulose composite aerogels

As is shown in Figure 11a, amount of AH NPs were coated on dense AH NPs@cellulose composite aerogels surface. Uniform SiO2 nanoparticles with an average size diameter about 100 nm were formed after modifying AH NPs@cellulose Composite Aerogels (Figure 11b). Both water and oil droplets can permeate through the AH NPs@cellulose Composite Aerogels immediately since the cellulose aerogels are highly permeable (Figure 11c). Interestingly, the modified AH NPs@cellulose composite aerogels exhibited excellent superamphiphobility (Figure 11d). The water contact angle (WCA) and the oil contact angle (OCA) for hexadecane are 159.7±1.3° and 149.7±1.5°, respectively. In addition, the modified samples not only have excellent resistance to oil and water, but also exhibit excellent uniform repulsion for strong acids and strong bases. Figure 11e showed optical images of oil, HCl (pH = 1), water and NaOH (pH = 14) droplets on the modified sample surface. These four droplets evenly showed the perfect spherical shapes, indicating the treated composite aerogels have strong resistance to moisture even for strong corrosive liquids. All of the modified AH NPs@cellulose composite aerogels samples exhibited excellent super-wettability, which is superior to cellulose aerogel (Figure 11f). These results all indicate that the modified AH NPs@cellulose composite aerogels exhibited excellent superamphiphobility. It is a very promising candidate for advanced engineering materials with anti-fouling functionality.[50,51]

Conclusions

AH NPs@cellulose composite aerogels with a homogeneous three-dimensional porous structure were fabricated successfully from cotton via in-situ synthesis of AH NPs in the cellulose gel scaffold. This is a facile, efficient, low cost, and

environmentally friendly process to achieve homogeneous distribution of flame retardants in cellulose aerogel and avoid nanoporous structure collapsed. AH NPs composite aerogels showed significant mechanical properties, and excellent flame retardancy and sound absorption. Moreover, superamphiphilic AH NPs composite cellulose aerogels were transferred into superamphiphobic by modifying them with silica nanoparticles together with heptadecafluorononanoic and fluoroalkyl silane, endowing them with super-antiwetting for both water and oil. The demonstrate process is facile, environmentally friendly, and with low cost. The resulting AH NPs@cellulose composite aerogels have excellent flame retardancy, are mechanically stronger, and displays high-efficiency sound-adsorption. The composite aerogels are promising candidates for advanced engineering materials with flame retardant, sound absorbing, thermal insulation and anti-fouling functionalities.[52]

Author Contributions

The manuscript was written through contributions of all authors. All authors have given approval to the final version of the manuscript.

Supporting Information

SEM images (Figure S1) and EDS (Figure S2) of residue after fire burning.

ACKNOWLEDGMENT

The authors thank the National Natural Science Foundation of China (21501127 and 51502185), Natural Science Foundation of Jiangsu Province of China (BK20140400), Nantong Science and Technology Project (GY12016030), Jiangsu Advanced Textile Engineering Center Project (Project No. SPPGO[2014]22), We also acknowledge the funds from the Priority Academic Program Development of Jiangsu Higher Education Institutions (PAPD), and Project for Jiangsu Scientific and Technological Innovation Team (2013).

REFERENCES

1. Pääkkö, M.; Vapaavuori, J.; Silvennoinen, R.; Kosonen, H.; Ankerfors, M.; Lindström, T.; Berglund, L. A.; Ikkala, O. Long and Entangled Native Cellulose I Nanofibers Allow Flexible Aerogels and Hierarchically Porous Templates for Functionalities. *Soft Matter* **2008**, *4*, 2492-2499. DOI: 10.1039/b810371b.
2. Korhonen, J. T.; Kettunen, M.; Ras, R. H.; Ikkala, O. Hydrophobic Nanocellulose Aerogels as Floating, Sustainable, Reusable, and Recyclable Oil Absorbents. *ACS Appl. Mater. Interfaces* **2011**, *3*, 1813-1816. DOI:10.1021/am200475b.
3. Chen, W.; Yu, H.; Li, Q.; Liu, Y.; Li, J. Ultralight and Highly Flexible Aerogels with Long Cellulose I Nanofibers. *Soft Matter* **2011**, *7*, 10360-10368. DOI: 10.1039/c1sm06179h.
4. Gao, X. D.; Huang, Y. D.; Zhang, T. T.; Wu, Y. Q.; Li, X. M. Amphiphilic SiO_2 Hybrid Aerogel: An Effective Absorbent for Emulsified Wastewater. *J. Mater. Chem. A* **2017**, *5*, 12856-12862. DOI: 10.1039/x0xx00000x.
5. Feng, J.; Nguyen, S. T.; Fan, Z.; Duong, H. M. Advanced Fabrication and Oil Absorption Properties of Super-hydrophobic Recycled Cellulose Aerogels. *Chem. Eng. J.* **2015**, *270*, 168-175.

DOI:10.1016/j.cej.2015.02.034.
6. Yu, R. M.; Shi, Y. Z.; Yang, D. Z.; Liu, Y. X.; Qu, J.; Yu, Z. Z. Graphene Oxide/Chitosan Aerogel Microspheres with Honeycomb Cobweb and Radially Oriented Microchannel Structures for Broad Spectrum and Rapid Adsorption of Water Contaminants. *ACS Appl. Mater. Interfaces* **2017**, *9*, 21809-21819. DOI: 10.1021/acsami.7b04655.
7. Liu, H. Z.; Geng, B. Y.; Chen, Y. F.; Wang, H. Y. Review on the Aerogel-type Oil Sorbents Derived from Nanocellulose. *ACS Sustain. Chem. Eng.* **2017**, *5*, 49-66. DOI: 10.1021/ acssuschemeng.6b02301.
8. Cai, H.; Sharma, S.; Liu, W.; Mu, W.; Liu, W.; Zhang, X.; Deng, Y. Aerogel Microspheres from Natural Cellulose Nanofibrils and Their Application as Cell Culture Scaffold. *Biomacromolecules* **2014**, *15*, 2540-2547. DOI:10.1021/bm5003976.
9. Naseri, N.; Poirier, J. M.; Girandon, L.; Fröhlich, M.; Oksman, K.; Mathew, A. P. 3-Dimensional Porous Nanocomposite Scaffolds Based on Cellulose Nanofibers for Cartilage Tissue Engineering: Tailoring of Porosity and Mechanical Performance. *RSC Adv.* **2016**, *6*, 5999-6007. DOI: 10.1039/x0xx00000x.
10. Si, Y.; Wang, X. Q.; Yan, C. C.; Yang, L.; Yu, J. Y.; Ding, B. Ultralight Biomass‐Derived Carbonaceous Nanofibrous Aerogels with Superelasticity and High Pressure‐Sensitivity. *Adv. Mater.* **2016**, *28*, 9512-9518. DOI: 10.1002/adma.201603143.
11. Xu, C.; Wei, Z.; Gao, H.; Bai, Y.; Liu, H.; Yang, H.; Lai, Y.; Yang, L. Bioinspired Mechano-Sensitive Macroporous Ceramic Sponge for Logical Drug and Cell Delivery. *Adv. Sci.* **2017**, *4*, 1600410. DOI: 10.1002/advs.201600410.
12. Cuce, E.; Cuce, P. M.; Wood, C. J.; Riffat, S. B. Toward Aerogel Based Thermal Superinsulation in Buildings: A Comprehensive Review. *Renew. Sust. Energy Rev.* **2014**, *34*, 273-299. DOI:10.1016/j.rser.2014.03.017.
13. Zhao, S.; Zhang, Z.; Sèbe, G.; Wu, R.; Rivera Virtudazo, R. V.; Tingaut, P.; Koebel, M. M. Multiscale Assembly of Superinsulating Silica Aerogels Within Silylated Nanocellulosic Scaffolds: Improved Mechanical Properties Promoted by Nanoscale Chemical Compatibilization. *Adv. Funct. Mater.* **2015**, *25*, 2326-2334. DOI: 10.1002/adfm.201404368.
14. Sadineni, S. B.; Madala, S.; Boehm, R. F. Passive Building Energy Savings: A Review of Building Envelope Components. *Renew. Sust. Energy Rev.* **2011**, *15*, 3617-3631. DOI:10.1016/j.rser.2011.07.014.
15. Wicklein, B.; Kocjan, A.; Salazar-Alvarez, G.; Carosio, F.; Camino, G.; Antonietti, M.; Bergström, L. Thermally Insulating and Fire-retardant Lightweight Anisotropic Foams Based on Nanocellulose and Graphene Oxide. *Nature Nanotech.* **2015**, *10*, 277-283. DOI: 10.1038/NNANO.2014.248.
16. Liang, S.; Zhang, L.; Li, Y.; Xu, J. Fabrication and Properties of Cellulose Hydrated Membrane with Unique Structure. *Macromol. Chem. Phys.* **2007**, *208*, 594-602. DOI: 10.1002/macp.200600579.
17. Wu, J.; Liang, S.; Dai, H.; Zhang, X.; Yu, X.; Cai, Y.; Zhang, L.; Wen, N.; B.; Jiang, Xu, J. Structure and Properties of Cellulose/chitin Blended Hydrogel Membranes Fabricated via a Solution Pre-gelation Technique. *Carbohydr. Polym.* **2010**, *79*, 677-684.DOI:10.1016/j.carbpol.2009.09.022.
18. Wan, C.; Li, J. Incorporation of Graphene Nanosheets into Cellulose Aerogels: Enhanced Mechanical, Thermal, and Oil Adsorption Properties. *Appl. Phys. A* **2016**, *122*, 105. DOI: 10.1007/s00339-016-9641-6.
19. Zhang, J.; Cao, Y.; Feng, J.; Wu, P. Graphene-Oxide-Sheet-Induced Gelation of Cellulose and Promoted Mechanical Properties of Composite Aerogels. *J. Phys. Chem. C* **2012**, *116*, 8063-8068. DOI:10.1021/jp2109237.
20. Zhang, L.; Li, X.; Wang, M.; He, Y.; Chai, L.; Huang, J.; Wang, H.; Wu, X.; Lai, Y. Highly Flexible and Porous Nanoparticle-Loaded Films for Dye Removal by Graphene Oxide–Fungus Interaction. *ACS Appl. Mater. Interfaces* **2016**, *8*, 34638-34647. DOI: 10.1021/acsami.6b10920.
21. Mao, J.; Ge, M.; Huang, J.; Lai, Y.; Lin, C.; Zhang, K.; Meng, K.; Tang, Y. Constructing Multifunctional MOF@rGO Hydro-/aerogels by the Self-assembly Process for Customized Water Remediation. *J. Mater. Chem. A* **2017**, *5*, 11873-11881. DOI: 10.1039/c7ta01343d.
22. Wang, L.; Sanchez-Soto, M.; Maspoch, M. L. Polymer/clay Aerogel composites with Flame

Retardant Agents: Mechanical, Thermal and Fire Behavior. *Mater. Des.* **2013**, *52*, 609-614. DOI: 10.1016/j.matdes.2013.05.096
Chen, H. B.; Chiou, B. S.; Wang, Y. Z.; Schiraldi, D. A. Biodegradable pectin/clay aerogels. *ACS Appl. Mater. Interfaces* **2013**, *5*, 1715-1721. DOI：10.1021 / am3028603.
23. Johnson, J. R.; Spikowski, J.; Schiraldi, D. A. Mineralization of clay/polymer aerogels: a bioinspired approach to composite reinforcement. *ACS Appl. Mater. Interfaces*, **2009**, *1*, 1305-1309. DOI: 10.1021/am9001919
24. Sun, H.; Schiraldi, D. A.; Chen, D.; Wang, D.; Soto, M. S. Tough polymer aerogels incorporating a conformal inorganic coating for low flammability and durable hydrophobicity. *ACS Appl. Mater. Interfaces* **2016**, *8*, 13051-13057. DOI: 10.1021/acsami.6b02829.
25. Viggiano, R. P.; Williams, J. C.; Schiraldi, D. A.; Meador, M. A. B. Effect of Bulky Substituents in the Polymer Backbone on the Properties of Polyimide Aerogels. *ACS Appl. Mater. Interfaces* **2017**, *9(9)*, 8287–8296. DOI: 10.1021/acsami.6b15440.
26. Isobe, N.; Sekine, M.; Kimura, S.; Wada, M.; Kuga, S. Anomalous Reinforcing Effects in Cellulose Gel-based Polymeric Nanocomposites. *Cellulose* **2011**, *18*, 327-333. DOI 10.1007/s10570-010-9487-6.
27. Carlsson, D. O.; Nyström, G.; Zhou, Q.; Berglund, L. A.; Nyholm, L.; Strømme, M. Electroactive Nanofibrillated Cellulose Aerogel Composites with Tunable Structural and Electrochemical Properties. *J. Mater. Chem.* **2012**, *22*, 19014-19024. DOI: 10.1039/c2jm33975g.
28. Azizi Samir, M. A. S.; Alloin, F.; Dufresne, A. Review of Recent Research into Cellulosic Whiskers, Their Properties and Their Application in Nanocomposite Field. *Biomacromolecules* **2005**, *6*, 612-626. DOI: 10.1021/bm0493685.
29. Bober, P.; Liu, J.; Mikkonen, K. S.; Ihalainen, P.; Pesonen, M.; Plumed-Ferrer, C.; Von, W. A.; Lindfors, T.; Xu, C. L.; Latonen, R. M. Biocomposites of Nanofibrillated Cellulose, Polypyrrole, and Silver Nanoparticles with Electroconductive and Antimicrobial Properties. *Biomacromolecules* **2014**, *15*, 3655-3663. DOI: 10.1021/bm500939x.
30. Olsson, R. T.; Azizi Samir, M. A. S.; Salazar-Alvarez, G.; Belova, L.; Ström, V.; Berglund, L. A.; Ikkala, O.; Gedde, U. W. Making Flexible Magnetic Aerogels and Stiff Magnetic Nanopaper Using Cellulose Nanofibrils as Templates. *Nature Nanotech.* **2010**, *5*, 584-588. DOI: 10.1038/NNANO.2010.155.
31. Han, Y.; Zhang, X.; Wu, X.; Lu, C. Flame Retardant, Heat Insulating Cellulose Aerogels from Waste Cotton Fabrics by in Situ Formation of Magnesium Hydroxide Nanoparticles in Cellulose Gel Nanostructures. *ACS Sustain. Chem. Eng.* **2015**, *3*, 1853-1859. DOI: 10.1021/acssuschemeng.5b00438.
32. Wang, L.; Sánchez-Soto, M. Green Bio-based Aerogels Prepared from Recycled Cellulose Fiber Suspensions. *RSC Adv.* **2015**, *5*, 31384-31391. DOI: 10.1039/c5ra02981c.
33. Joni, I. M.; Nishiwaki, T.; Okuyama, K.; Isoi, S.; Kuribayashi, R. Enhancement of the Thermal Stability and Mechanical Properties of a PMMA/aluminum Trihydroxide Composite Synthesized via Bead Milling. *Powder Technol.* **2010**, *204*, 145-153. DOI: 10.1016/j.powtec.2010.07.032.
34. Könnicke, D.; Kühn, A.; Mahrholz, T.; Sinapius, M. Polymer Nanocomposites Based on Epoxy Resin and ATH as a New Flame Retardant for CFRP: Preparation and Thermal Characterisation. *J. Mater. Sci.* **2011**, *46*, 7046-7055. DOI 10.1007/s10853-011-5673-7.
35. Witkowski, A.; Ste, A. A.; Hull, T. R. The Influence of Metal Hydroxide Fire Retardants and Nanoclay on the Thermal Decomposition of EVA. *Polym. Degrad. Stabil.* **2012**, *97*, 2231-2240. DOI: 10.1016/j.polymdegradstab.2012.08.003.
36. Liu, H.; Huang, J.; Li, F.; Chen, Z.; Zhang, K. Q.; Al-Deyab, S. S.; Lai, Y. Multifunctional Superamphiphobic Fabrics with Asymmetric Wettability for One-way Fluid Transport and Templated Patterning. *Cellulose* **2017**, *24*, 1129-1141. DOI 10.1007/s10570-016-1177-6.
37. Oréfice, R. L.; Vasconcelos, W. L. Sol-gel transition and structural evolution on multicomponent gels derived from the alumina-silica system. *J. Sol-Gel Sci.Tech.***1997**, *9*, 239-249.
38. Savini, G.; Dappe, Y. J.; Öberg, S.; Charlier, J. C.; Katsnelson, M. I.; Fasolino, A. Bending modes, elastic constants and mechanical stability of graphitic systems. *Carbon* **2011**, *49*, 62-69. DOI:

10.1016/j.carbon.2010.08.042.
39. Gu, J.; Sansoz, F. Role of cone angle on the mechanical behavior of cup-stacked carbon nanofibers studied by atomistic simulations. *Carbon* **2014**, *66*, 523-529. DOI: 10.1016/j.carbon.2013.09.029.
40. Si, Y.; Yu, J. Y.; Tang, X. M.; Ge, J. L.; Ding, B. Ultralight Nanofibre-assembled Cellular Aerogels with Superelasticity and Multifunctionality. *Nature Commun.* **2014**, *5*, 5802. DOI: 10.1038/ncomms6802.
41. Kashiwagi, T.; Du, F.; Douglas, J. F.; Winey, K. I.; Harris Jr, R. H.; Shields, J. R. Nanoparticle networks reduce the flammability of polymer nanocomposites. *Nature Mater.* **2005**, *4,* 928-933. DOI: 10.1038/nmat1502.
42. Wang, B.; Zhou, K.; Jiang, S.; Hu, Y.; Gui, Z. The Application of Transition Metal Molybdates ($AMoO_4$, A = Co, Ni, Cu) as Additives in Acrylonitrile-butadiene-styrene with Improved Flame Retardant and Smoke Suppression Properties. *Polym. Adv. Technol.* **2014**, *25*, 1419-1425. DOI: 10.1002/pat.3380.
43. Wu, N.; Yang, R. Effects of Metal Oxides on Intumescent Flame‐Retardant Polypropylene. *Polym. Adv. Technol.* **2011**, *22*, 495-501. DOI: 10.1002/pat.1539.
44. Li, W.; Hou, Y.; Yang, F.; Wu, W. Production of Benzene Carboxylic Acids and Small-Molecule Fatty Acids from Lignite by Two-Stage Alkali-Oxygen Oxidation. *Ind. Eng. Chem. Res.* **2017**, *56*, 1971-1978. DOI: 10.1021/acs.iecr.6b04562.
45. Kashiwagi, T.; Grulke, E.; Hilding, J.; Groth, K..; Harris, R.; Butler, K.; Shields, J.; Kharchenko, S.; Douglas, J. Thermal and flammability properties of polypropylene/carbon nanotube nanocomposites. *Polymer* **2004**, *45*, 4227-4239.DOI: 10.1016/j.polymer.2004.03.088.
46. Kashiwagi, T.; Du, F.; Winey, K. I.; Groth, K. M.; Shields, J. R.; Bellayer, S. P.; Kim, H.; Douglas, J. F. Flammability properties of polymer nanocomposites with single-walled carbon nanotubes: effects of nanotube dispersion and concentration. *Polymer* **2005**, *46*, 471-481.DOI: 10.1016/j.polymer.2004.10.087.
47. Schartel, B.; Pötschke, P.; Knoll, U.; Abdel-Goad, M. Fire behaviour of polyamide 6/multiwall carbon nanotube nanocomposites. *Eur. Polym. J.* **2005**, *41*, 1061-1070. DOI: 10.1016/j.eurpolymj.2004.11.023.
48. Xie, H.; Yang, W.; Yuen, A. C. Y.; Xie, C.; Xie, J.; Lu, H.; Yeoh, G. H. Study on flame retarded flexible polyurethane foam/alumina aerogel composites with improved fire safety. *Chem. Eng. J.*, **2017**, *311*, 310-317. DOI: 10.1016/j.cej.2016.11.110.
49. Liu, H.; Huang, J.; Chen, Z.; Chen, G.; Zhang, K.; Al-Deyab, S.; Lai, Y. Robust translucent superhydrophobic PDMS/PMMA film by facile one-step spray for self-cleaning and efficient emulsion separation. *Chem. Eng. J.*, **2017**, *330*, 26-35. DOI: 10.1016/j.cej.2017.07.114.
50. Cao, C.; Ge, M.; Huang, J.; Li, S.; Deng, S.; Zhang, S., Chen, Z.; Zhang, K.; Al-Deyab, S.; Lai, Y. Robust fluorine-free superhydrophobic PDMS-ormosil@fabrics for highly effective self-cleaning and efficient oil–water separation. *J. Mater. Chem. A* **2016**, *4*, 12179-12187. DOI: 10.1039/c6ta04420d.
51. Baetens, R.; Jelle, B. P.; Gustavsen, A. Aerogel Insulation for Building Applications: A State-of-the-art Review. *Energy Building* **2011**, *43*, 761-769. DOI: 10.1016/j.enbuild.2010.12.012.

Table 1. The MCC results of cellulose aerogel and AH NPs@cellulose composite aerogels.

Sample	TTI (s)	THR (kJ/g)	PHRR (W/g)	T_{PHRR} (°C)	TI_{PHRR} (s)	Residue (%)
C0	17	13.2	280	346	345	8.9
C1	20	5.8	100	310	309	17.2
C2	25	4.7	61	289	291	26.3
C3	23	3.1	45	257	256	46.6
C4	26	1.6	22	233	232	63.4

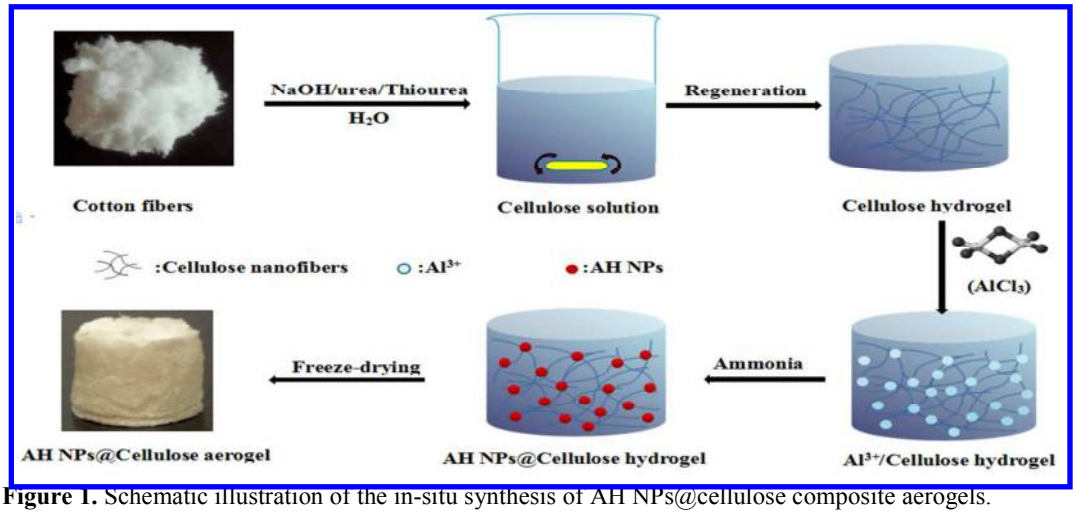

Figure 1. Schematic illustration of the in-situ synthesis of AH NPs@cellulose composite aerogels.

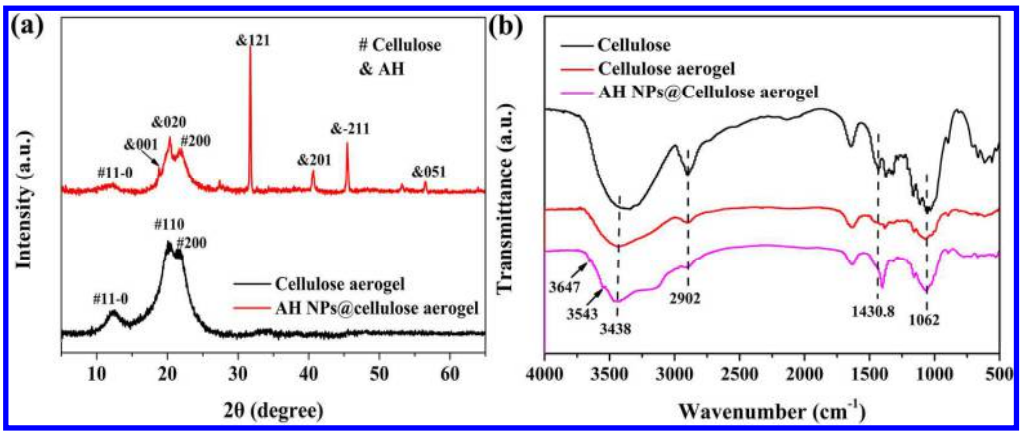

Figure 2. XRD patterns (a) and FT-IR spectra (b) of cellulose aerogel and AH NPs@cellulose composite aerogels.

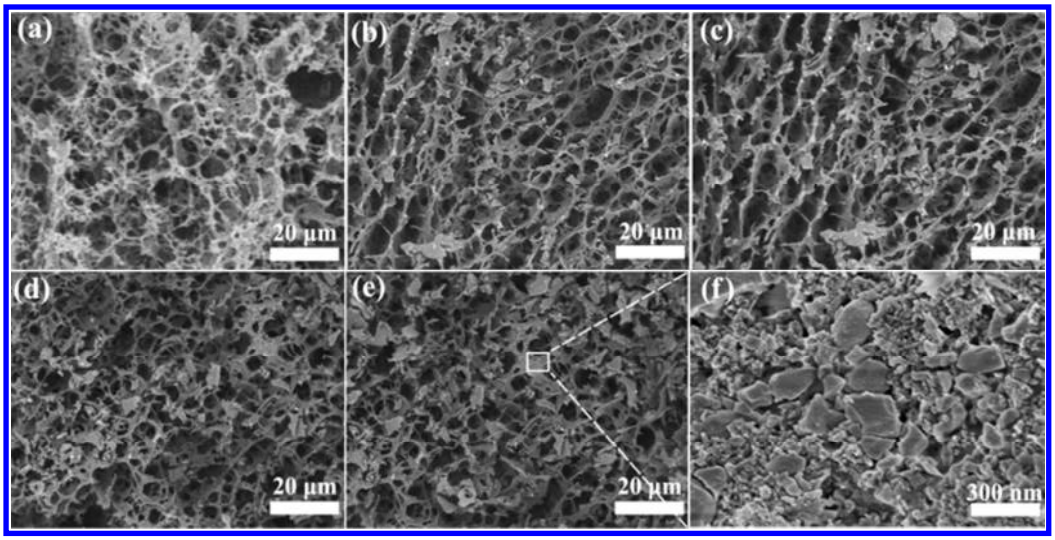

Figure 3. SEM images of cellulose aerogel C0 (a) and AH NPs@cellulose composite aerogels: C1 (b), C2 (c), C3 (d), and C4 (e, f).

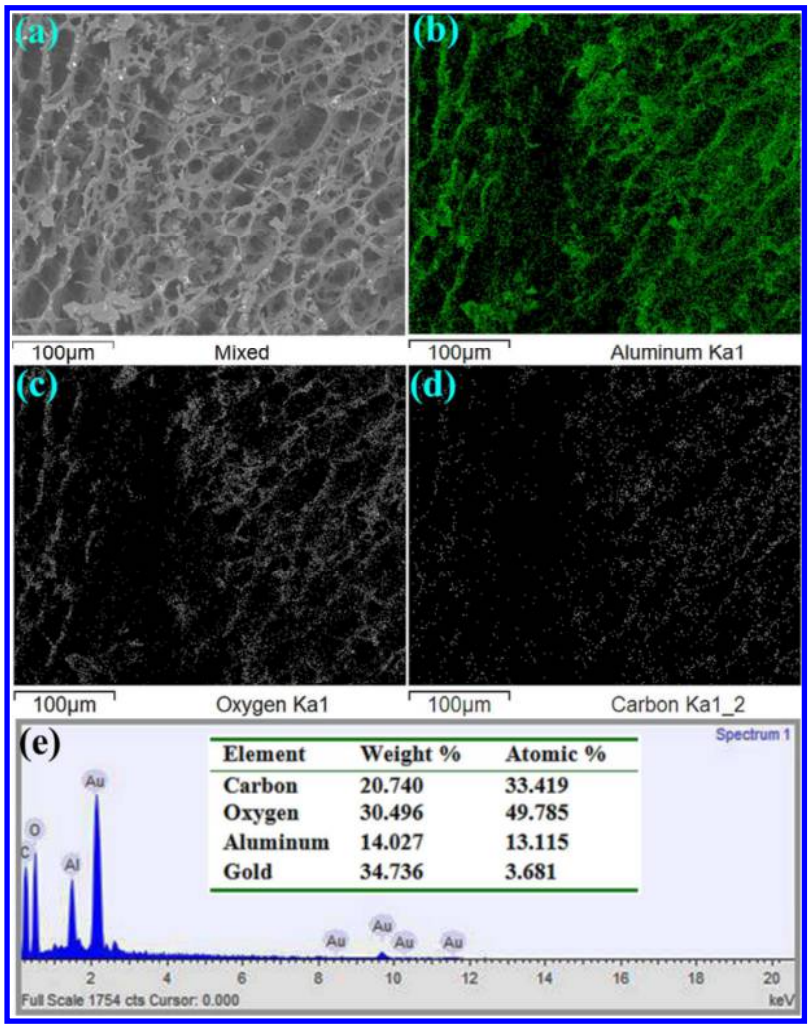

Figure 4. The scanning images of AH NPs@cellulose composite aerogels (a), elemental mapping of aluminum (b), oxygen (c), carbon (d), and EDS spectrum (e).

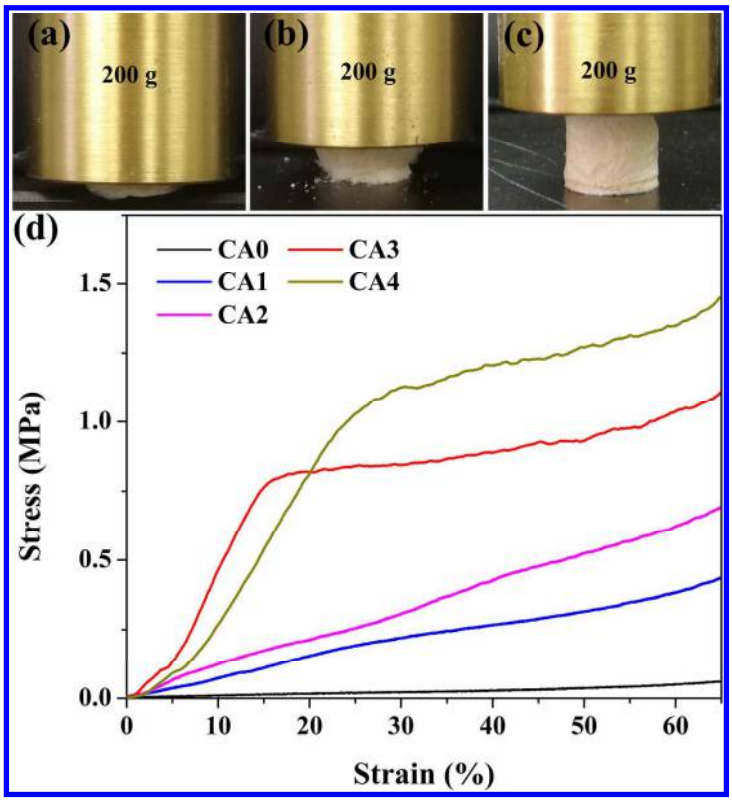

Figure 5. Optical images of CA0 (a), CA1 (b) and CA4(c) cellulose aerogels compression performance.

Compression stress-strain curves (d) of cellulose aerogel and AH NPs@cellulose composite aerogels.

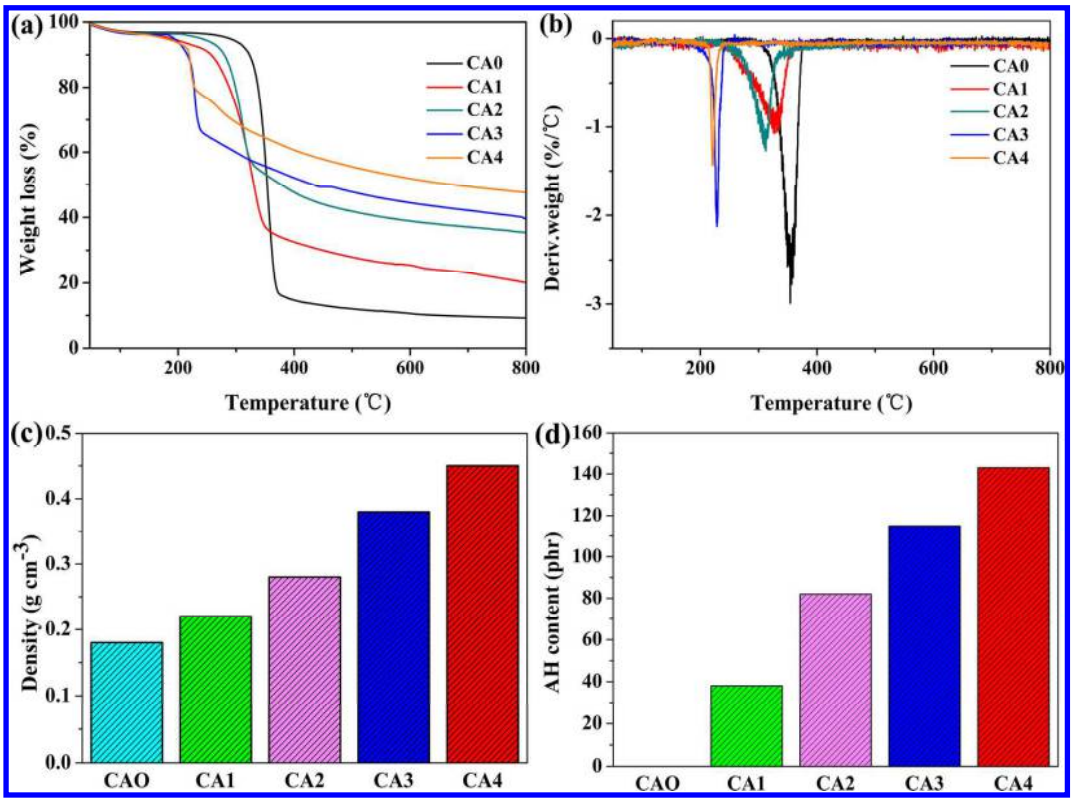

Figure 6. TGA (a) and DTG (b) curves of cellulose aerogel and AH NPs@cellulose composite aerogels. (c) Density of cellulose aerogel and AH NPs@cellulose composite aerogels. (d) AH NPs content in the composite aerogels (phr: parts per hundred parts of cellulose).

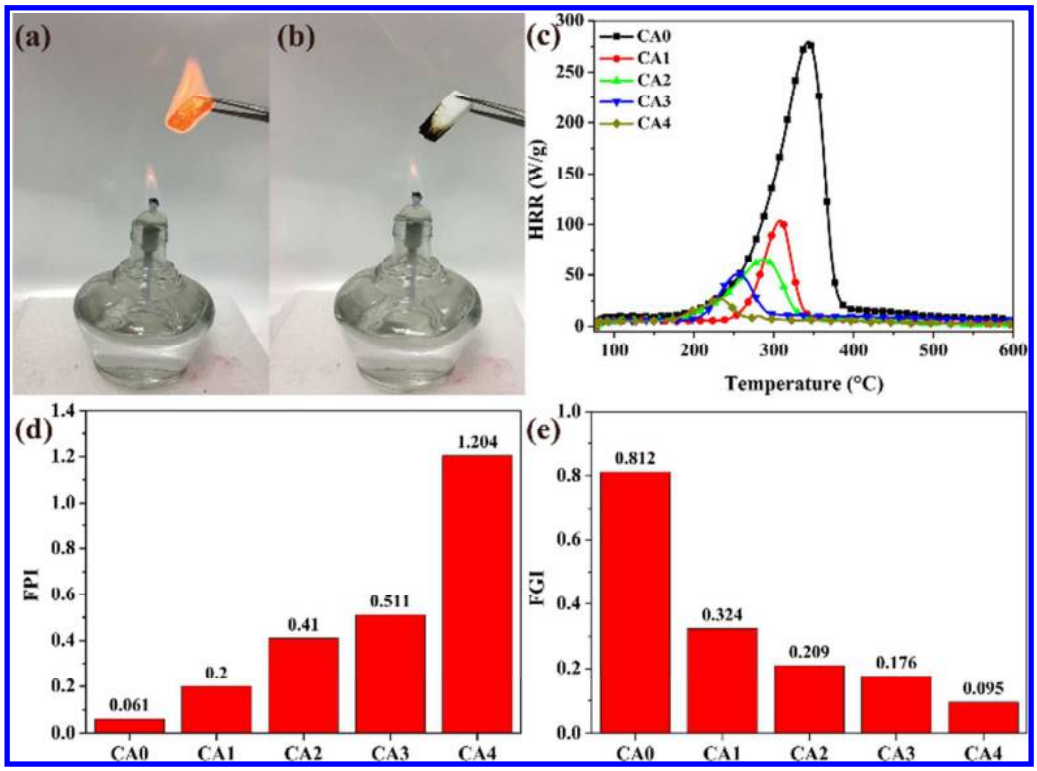

Figure 7. Optical images of cellulose aerogels (a) and AH NPs@cellulose composite aerogels (b) captured after ignition by an alcohol burner. HRR curves (c) of cellulose aerogel and AH NPs@cellulose composite aerogels measured by MCC. MCC fire performance index (d) and fire growth index (e) for all samples.

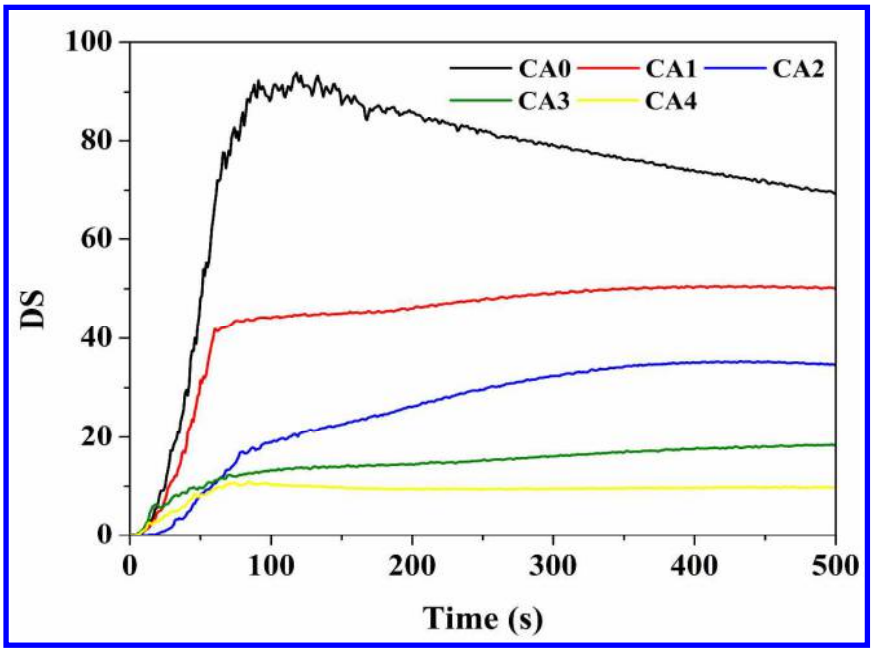

Figure 8. Smoke density of different kinds of composte aerogels.

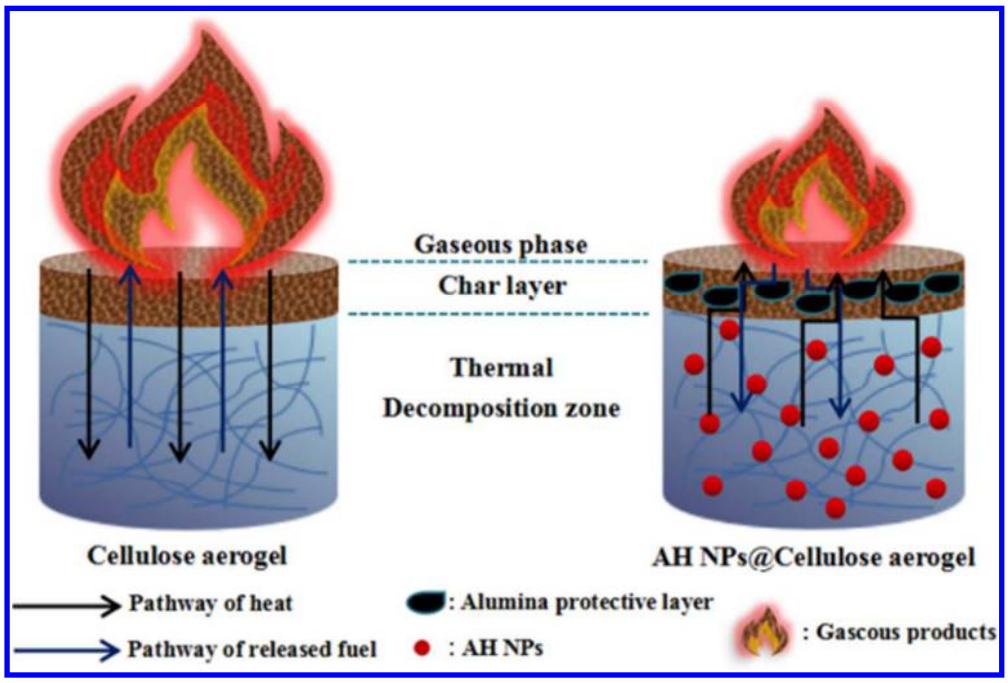

Figure 9. Proposed mechanisms of the thermal stability flame retardancy of cellulose aerogel and its composites.

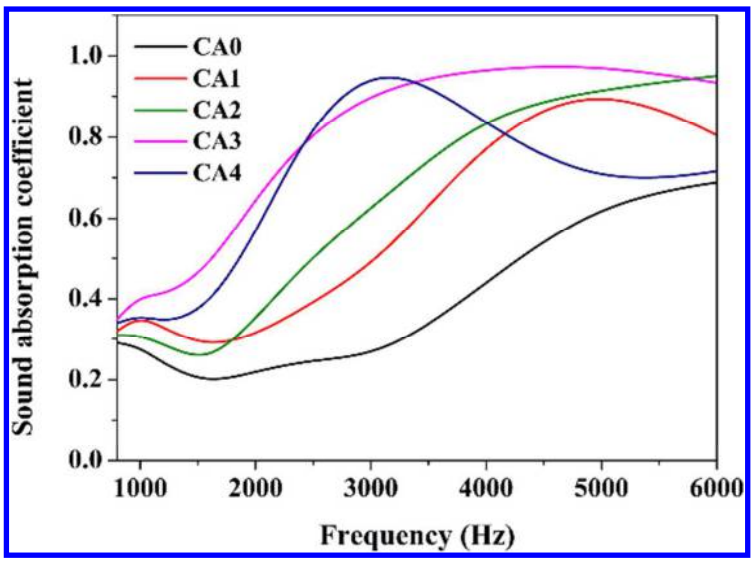

Figure 10. The sound-absorbing performance testing of samples.

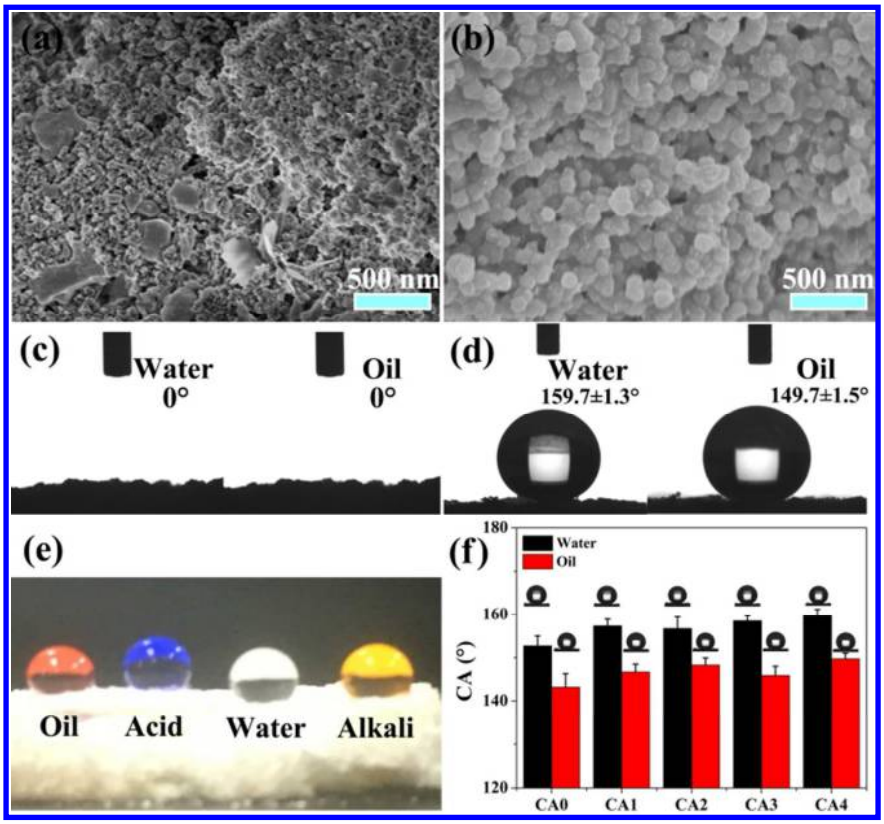

Figure 11. SEM image of AH NPs@cellulose composite aerogels (a), and the modified AH NPs@cellulose composite aerogels (b). Water and oil CA of AH NPs@cellulose composite aerogels (c) and the modified AH NPs@cellulose composite aerogels (d); (e) The optical images of the oil, HCl solution (pH=1), water, and NaOH solution (pH=14) droplets on the superamphiphobic AH NPs@cellulose composite aerogels surface kept nearly spherical shapes; (f) The water and oil contact angle of the modified AH NPs@cellulose composite aerogels.

For Table of Contents Use Only:

Mechanical resistant cellulose-based aerogels with excellent flame retardant, high-efficiency sound-adsorption and super-antiwetting abilities are rationally constructed for sustainable and green multifunctional building materials.